Food Hydrocolloids 135 (2023) 108192

Contents lists available at ScienceDirect

Food Hydrocolloids

journal homepage: www.elsevier.com/locate/foodhyd

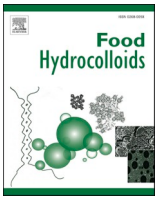

Sargassum inspired, optimized calcium alginate bioplastic composites for food packaging

Akeem Mohammed [a], Andre Gaduan [b], Pooran Chaitram [a], Anaadi Pooran [a], Koon-Yang Lee [b,**], Keeran Ward [c,*]

[a] Department of Chemical Engineering, University of the West Indies, St. Augustine, Trinidad, WI, USA
[b] Department of Aeronautics and Institute for Molecular Science and Engineering, Imperial College London, South Kensington Campus, SW7 2AZ, London, UK
[c] School of Chemical and Process Engineering (SCAPE), University of Leeds, Leeds, LS2 9JT, UK

ARTICLE INFO

Keywords:
Sargassum natans
Composite bioplastics
Biodegradable films
RSM
Food packaging
Alginate

ABSTRACT

Plastic pollution, more specifically from food packaging and containers which account for the largest share of 36% of current plastic production, is one of the greatest threats to the natural environment and human health. Thus, the development of alternative renewable plastics are needed to complement a circular economy and reduce resource depletion. Seaweeds have been known to possess good film forming properties ideal for bioplastic production, and *Sargassum natans*-an invasive brown seaweed which has been inundating the shores of the Caribbean, has been shown to be an excellent candidate. This study presents, for the first time, the development of a novel optimized biodegradable alginate composite bioplastic as an alternative to traditional plastic packaging. The optimization process was carried out using Response Surface Methodology (RSM) resulting in a formulation of 6 wt% alginate, 0.263 wt% starch, 0.35 wt% CMC, 0.065 g/g sorbitol and 0.025 g/g PEG 200- with ultra-high oxygen barrier (OP - 0.2 cm^3 μm m^{-2} d^{-1} kPa^{-1}), good water vapor barrier (WVP - 2.18 × 10^{-12} g m/m^2 s Pa) and high tensile modulus (*E* - 3.93 GPa)- with no migration of additives into a simulated aqueous food system in 10 days. Furthermore, composite films were found to fully degrade in 14 days and possessed better OP, higher WVP and comparable material properties to HDPE, PET and PLA. Ultimately, our results support alginate composite films as a viable alternative for food packaging best fitted for low moisture environments-encouraging the use of renewable materials for packaging innovation and supporting UNSDGs.

1. Introduction

Plastics, mainly composed of synthetic polymers, have a variety of uses and are integral to everyday life. They contribute to economic growth, but their current production and use patterns are primary drivers of natural resource depletion, waste, and environmental degradation. Plastics also have very slow decomposition rates and as such, pose several environmental concerns as plastic particles have spread across the world's oceans contributing largely to contamination in the food chain (Pilz, Brandt, & Fehringer, 2010, pp. 1–45; Zygmunt, 2007). Many food products require packaging to ensure their quality, safety, and security. Polymer-based multilayer packaging materials are frequently utilized to combine the properties of various polymers. This technique results in packaging solutions with specific functionality with high tensile modulus (*E*), low oxygen permeation (OP) and low water vapor permeation (WVP) rates to adequately protect delicate food goods and hence extend shelf life. Multilayer food packaging is especially under pressure since it combines various materials such as polymers, paper, aluminum, and organic or inorganic coatings (Kaiser, Schmid, & Schlummer, 2018; Marrone & Tamarindo, 2018). The components of multi-material multilayer structures are layered to make flexible packaging (pouches, bags, shrink films, and other pliable products) or rigid packaging (pouches, bags, shrink films, and other stiff packaging such as trays, cups, containers and plastic sheets) (Soares, Ek, Östmark, Gällstedt, & Karlsson, 2022).

However, these food packaging face many challenges at its end-of-life- due to limited sorting and recyclability within existing waste management infrastructure. Currently, solutions for recyclable films have been achieved for those based on polyolefins (polyethylene (PE) and polypropylene (PP)) but require the restriction of certain polymers

* Corresponding author.
** Corresponding author.
E-mail addresses: koonyang.lee@imperial.ac.uk (K.-Y. Lee), k.r.ward@leeds.ac.uk (K. Ward).

https://doi.org/10.1016/j.foodhyd.2022.108192
Received 26 July 2022; Received in revised form 21 September 2022; Accepted 26 September 2022
Available online 30 September 2022

such as polyamide (PA) and polyethylene terephthalate (PET) (Van Eygen, Laner, & Fellner, 2018). The fact that increasing the recyclability of multilayer films sometimes means lowering packaging efficiency poses a challenge. Thus, there is a need for future flexible and rigid packaging solutions with emphasis on sustainability and end-of-life options that have a clear benefit to the environment and can contribute to a circular economy.

For these reasons, the development and production of biodegradable materials as an alternative to conventional plastics, with controlled properties for food applications has been the subject of great research due to their renewability, compostability and biodegradability. A further driver for these alternate materials is the establishment of the United Nations' 17 sustainable development goals (SDG's). Bioplastics allow for the innovation and development of a sustainable option by using renewable feedstocks such as cellulose, algae, lignin while offering a wider scope for end of life products and future packaging solutions.

Within the past decade, Trinidad and Tobago and by extension, the Caribbean and Latin America, has seen massive onslaughts of *Sargassum natans* brown seaweed onto its shores. This tremendous influx negatively impacts the economic, social and environmental aspects of the country (Johnson, Ko, Franks, Moreno, & Sanchez-Rubio, 2012; Langin, 2018; Resiere et al., 2018). However, this *Sargassum* contains a valuable hydrocolloid in the form of sodium alginate with film-forming capabilities. Bioplastics specifically created from macro-algae are easily cultivated in natural environments with no pesticides or fertilizers, does not compete with food sources, can be harvested all year round, able to grow in a wide range of environments and reduce CO_2 emissions and promote greenhouse gas uptake (Chia, Ying Tang, Khoo, Kay Lup, & Chew, 2020; Zeller, Hunt, Jones, & Sharma, 2013).

Nevertheless, bioplastics prepared from alginates are limited since they exhibit high stiffness, high brittleness, low deformability and moisture sensitivity when compared to conventional synthetic plastics. However, these problems can be remediated through the use of composite technology with other natural polymers, plasticizers and reinforcement materials (Avella et al., 2007). The use of alginate as a bioplastic, coupled with secondary biopolymers (Azeredo, Miranda, Rosa, Nascimento, & de Moura, 2012; Murad, Karim, Bhat, Uthumporn, & Chew, 2011), different concentrations of plasticizers (Jost, Kobsik, Schmid, & Noller, 2014) and different crosslinking treatments (Murad et al., 2011; Rhim, 2004) have been reported in literature. However, there is very little research that has been carried out to investigate the interactive relationships of blended alginate composites on material and barrier properties. This relationship among different factors and their effects can be investigated and optimized through the use of Design of Experiments (DOE).

Limited optimization studies have been carried out on the fabrication of alginate bioplastic films (Lim, Hii, Chee, & Wong, 2018; Wang, Auty, & Kerry, 2010) and to the best of our knowledge, no mixed plasticizer-mixed polymer bioplastic film has ever been fabricated from alginate derived from *S.natans*. Thus, this study presents for the first time, the optimization and development of a novel biodegradable alginate composite derived from *Sargassum* seaweed for food packaging. Our novel alginate composite bioplastic showcases enhanced oxygen resistance and comparable material properties as conventional synthetic and bioplastic alternatives, compatible with low moisture environments. Furthermore, this study illustrates a circular process, whereby pelagic *Sargassum* biomass can be utilized and valorized into high-value packaging-while informing and providing innovative modeling approaches to alternative food packaging.

2. Materials and methods

2.1. Materials

A blend of sodium alginate was used which comprised of alginate extracted *Sargassum natans* seaweed from local bays in East Trinidad and from Manugel DMB (donated by FMC Biopolymer). Different concentration of plasticizers and reinforcement material were added to make the casting solutions. Casting solutions comprised of varying concentrations of carboxymethyl cellulose, CMC (Sigma Aldrich, Mw 700,000), potato starch (SDFCL, purity >90%), sorbitol (Sigma Aldrich, purity >98%) and polyethylene glycol, (PEG200) (Sigma Aldrich). "Calcium chloride dihydrate (Sigma Aldrich, purity >99%) was used as the crosslinking agent." Humidity control was done using magnesium nitrate hexahydrate, $Mg(NO_3)_2.6H_2O$ (Sigma Aldrich, purity >99%). Disintegration study was done using simulated compost comprising of mature compost (donated by a local supplier, San Fernando Trinidad), sawdust, rabbit food (Sunburst, 13% minimum crude protein), corn starch (Sincere's Food Manufacturing), sugar, corn oil (Wesson) and urea (Nutrien, Granular Agricultural Grade 46-0-0). For comparison purposes, commercial films such as polyethylene terephthalate, PET (Goodfellow Cambridge Limited, 0.05 mm thickness, biaxially oriented), polylactic acid, PLA (Goodfellow Cambridge Limited, 0.05 mm thickness, biaxially oriented) and high-density polyethylene, HDPE (Goodfellow Cambridge Limited, 0.01 mm thickness) were used.

2.2. Experimental design

Preliminary work into pure alginate films fabricated from *Sargassum* derived alginate have been found to possess high brittleness and poor workability. These problems need to be remediated in order to fabricate a feasible bioplastic comparable to synthetic and biopolymer alternatives. Plasticizers and reinforcement materials are additives that can be added into the alginate matrix to alleviate such problems. Preliminary scoping of composite films were fabricated using a one factor at a time approach. The additives which gave the most synergistic effects with the alginate matrix were sorbitol and PEG 200 as plasticizers and starch and CMC as reinforcement materials.

To study the effects of the varying concentrations of starch, CMC, sorbitol and PEG 200 on *E*, WVP and OP of the alginate bioplastic, a Central Composite Design (CCD) was employed. The experimental domain was also chosen based on preliminary experimental scoping and the CCD at five levels (-α,-1, 0, 1, α) are presented in Table 1. CCD was chosen as the RSM design as it enabled the use of additional concentrations called 'axial points' to estimate curvature. This design allows for the constant prediction of variance at levels investigated due to their equal proximity to the center point (Myers, Montgomery, & Anderson-Cook, 2009).

The complete design consisted of 30 experimental runs (16 factorial points, 8 axial points and 6 replicates at the center point) carried out in a random order as shown in Table 2. To predict the optimal concentrations for the bioplastic formulation from the data points, a second-order polynomial model was fitted to according to Equation **(1)**:

$$Y = \beta_0 + \sum_{j=i}^{k} \beta_i x_i + \sum_{j=i}^{k} \beta_{ii} x_i^2 + \sum \sum_{i<j}^{k} \beta_{ij} x_i x_j \quad (1)$$

Where Y is the response function, β_0,β_i,β_{ii} and β_{ij} are coefficients for the intercept, linear, quadratic and interactive terms respectively; x_i, x_i^2 and $x_i x_j$ represent linear, quadratic and interactive terms of coded independent variables respectively and k represents the number of inde-

Table 1
Parameters and coded levels used in the CCD.

Experimental variables		Factor level				
Un-coded	Coded	-α	−1	0	1	α
Starch (wt. %)	A	0.05	0.2	0.35	0.5	0.65
CMC (wt. %)	B	0.05	0.15	0.25	0.35	0.45
Sorbitol (g/g)*	C	0.005	0.025	0.045	0.065	0.085
PEG 200 (g/g)*	D	0.005	0.025	0.045	0.065	0.085

Note: *(g/g) - Corresponds to gram/gram of alginate used.

Table 2
Un-coded CCD factors, model responses and raw tensile data.

	Independent variables				Responses			Tensile data	
Run	A	B	C	D	WVP ($\times 10^{-12}$ g m/m^2 s Pa)	OP (cm^3 μm m^{-2} d^{-1} kPa^{-1})	*E* (GPa)	σ (MPa)	ε (%)
1	0.350	0.250	0.045	0.045	2.83	0.10	1.48	33.89 ± 4.58	14.95 ± 7.76
2	0.350	0.450	0.045	0.045	2.34	0.07	2.52	48.4 ± 4.98	8.74 ± 1.46
3	0.200	0.150	0.025	0.065	2.27	0.27	2.49	49.41 ± 5.65	9.61 ± 3.55
4	0.350	0.250	0.005	0.045	2.80	0.60	2.61	50.13 ± 8.65	10.65 ± 4.6
5	0.050	0.250	0.045	0.045	2.03	0.14	2.77	57.03 ± 4.47	8.14 ± 2.13
6	0.650	0.250	0.045	0.045	3.55	0.08	3.08	54.17 ± 6.06	7.07 ± 2.38
7	0.350	0.250	0.045	0.045	2.40	0.11	1.82	54.53 ± 10.34	6.80 ± 3.19
8	0.200	0.150	0.065	0.065	1.84	0.18	3.30	60.08 ± 2.74	6.74 ± 1.93
9	0.500	0.350	0.065	0.025	2.34	0.80	3.38	62.88 ± 4.02	8.55 ± 1.07
10	0.200	0.350	0.025	0.065	1.91	0.17	3.92	63.75 ± 3.59	7.23 ± 2.48
11	0.500	0.350	0.065	0.065	1.94	0.22	3.17	53.36 ± 6.35	7.90 ± 3.16
12	0.500	0.350	0.025	0.025	1.74	0.21	3.98	63.41 ± 7.16	5.87 ± 1.92
13	0.350	0.250	0.045	0.045	2.99	0.10	1.02	23.01 ± 3.04	21.88 ± 3.42
14	0.350	0.250	0.045	0.045	2.90	0.10	1.79	38.58 ± 3.37	17.58 ± 1.99
15	0.200	0.150	0.025	0.025	2.18	0.47	1.41	37.41 ± 8.66	7.90 ± 3.16
16	0.350	0.250	0.045	0.045	2.62	0.10	1.64	35.21 ± 2.26	16.72 ± 2.7
17	0.350	0.050	0.045	0.045	2.62	0.13	1.12	37.98 ± 2.84	16.79 ± 1.03
18	0.200	0.150	0.065	0.025	1.45	0.07	1.98	40.58 ± 5.41	8.94 ± 2.54
19	0.500	0.150	0.025	0.065	2.71	0.03	2.35	52.14 ± 4.38	9.33 ± 2.27
20	0.350	0.250	0.045	0.045	2.50	0.10	1.82	44.39 ± 4.04	14.77 ± 3.61
21	0.350	0.250	0.045	0.005	1.70	0.12	3.89	70.00 ± 3.28	8.19 ± 2.16
22	0.350	0.250	0.085	0.045	1.72	0.06	6.14	91.25 ± 5.89	4.73 ± 0.66
23	0.500	0.150	0.025	0.025	1.65	0.09	3.28	64.4 ± 4.58	8.18 ± 2.06
24	0.200	0.350	0.065	0.065	2.19	0.04	4.76	72.15 ± 4.92	5.93 ± 1.52
25	0.350	0.250	0.045	0.085	3.06	0.95	2.75	49.6 ± 4.17	9.78 ± 3.31
26	0.200	0.350	0.025	0.025	1.64	0.14	3.24	58.21 ± 1.86	10.09 ± 1.65
27	0.500	0.150	0.065	0.065	1.10	0.08	5.17	83.42 ± 2.54	5.15 ± 0.55
28	0.200	0.350	0.065	0.025	2.00	0.89	4.49	75.75 ± 3.79	6.97 ± 0.60
29	0.500	0.150	0.065	0.025	2.76	0.09	2.82	56.48 ± 4.84	12.76 ± 2.75
30	0.500	0.350	0.025	0.065	2.23	0.57	3.03	54.88 ± 3.41	10.30 ± 1.60

pendent parameters (k = 4).

2.3. Alginate bioplastic composite preparation

The casting solutions were prepared using the combinations stipulated in Table 2 for all 30 runs. The wt. % of the alginate was kept constant for all experiments and comprised of a blend consisting of 2 wt % alginate extracted from *Sargassum natans* and 4 wt % Manugel (commercial brand) while the additives varied. The detailed extraction methodology can be found in the **Supplementary Material**. Casting solutions were thermo-mixed using a stirrer and hotplate (VWR 371, USA) for 2 h at 80 °C adapted from Gao, Pollet, and Avérous (2017a) and homogenized solutions were left to stand overnight to de-aerate. A calcium chloride bath was prepared using a 1:1 ratio of wt. % alginate to calcium chloride. The casting solution was poured onto poly methyl methacrylate (PMMA) plates and a 1 mm film was cast using a casting machine (Elcometer 4340 Automatic Film Applicator, USA). The plate was immersed into the calcium chloride bath for 1 h after which the film was detached and washed to remove any residual calcium chloride on the surface. Subsequently, the film was dried at 30 °C for 24 h (Ho et al., 2020; Li, He, Huang, Li, & Chen, 2015) in an oven (Thermo Fisher Scientific 3524, USA). The films were then stored in a desiccator at 0%

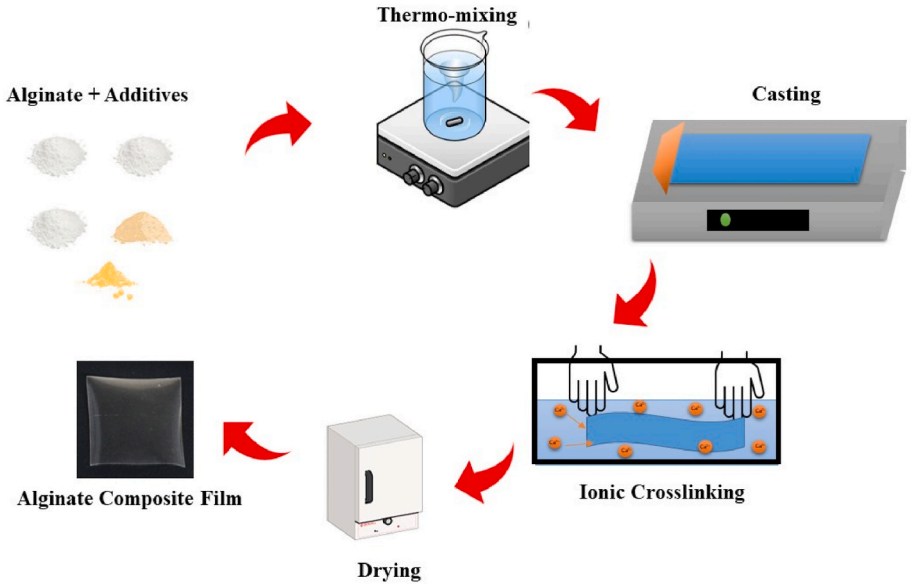

Fig. 1. Schematic of the bioplastic formulation to form calcium alginate composite films.

RH prior to being conditioned for testing. Fabricated and commercial films were conditioned at both 0% and 50 ± 2% relative humidity. Films conditioned at 50% RH were placed in a sealed chamber containing a saturated solution of magnesium nitrate hexahydrate, $Mg(NO_3)_2.6H_2O$ (O'Brien, 1948), for a minimum of 3 days prior to testing. Fig. 1 shows a schematic of the bioplastic formulation to form calcium alginate composite films.

2.4. Water vapor permeability (WVP)

This was done in accordance with ASTM E95-96 (1995) method. Desiccant (silica gel) was dried in an oven (Thermo Electron Cooperation 6542) for 30 min at 100 °C. A test cup (68–3000 EZ-Cup Vapometer Cup, Thwing-Albert Instrument Company USA) was filled with 3 mm of distilled water. A film of diameter 6 mm and thickness 80 μm was attached to the dish, sealed and the initial mass of the dishes was weighed (Adventurer Pro, USA). The thickness of the films was taken at 10 randomized points and an average found. The cup was placed into the desiccator with the dried desiccant and weighed at 30 min intervals for 6 h. The water vapor transmission rate was calculated using Equations (2)–(4) in duplicate;

$$Water\ Vapor\ Transmission, WVT = \frac{\left(\frac{G}{t}\right)}{A} \tag{2}$$

Where G is the mass change of water in dish (g), t is the time (h), G/t represents the slope of the straight line, (g/h) and A is the test area (cup mouth area) of 0.0032 m^2.

$$Permeance, P = \frac{WVT}{\Delta P} = \frac{WVT}{S(R_1 - R_2)} \tag{3}$$

$$Water\ Vapor\ Permeability, WVP = P \times Avg\ thickness \tag{4}$$

Where ΔP is the vapor pressure difference (mmHg), S is the Saturation Vapor Pressure at test temp (22 °C) taken as 20.941 mmHg (Liley, Thomson, Friend, Daubert, & Buck, 2008), R_1 represents the relative humidity at the source expressed as a fraction (test chamber for desiccant method; in the dish for water method), 100% and R_2 represents the relative humidity at the vapor sink expressed as a fraction, 0%.

2.5. Oxygen permeability (OP)

The OP was carried out in accordance with ASTM D3985-17 (2017) method. A film of 6 cm in diameter and thickness of 80 μm was cut from the dried film. The alginate bioplastic film was loaded into an oxygen permeation cell (PreSens, Germany) and sealed with vacuum grease. The bottom chamber was first purged with a stream of nitrogen gas followed by the top compartment. The bottom chamber was then charged with a stream of pure oxygen gas and the system was closed. An integrated electrochemical oxygen sensor (PSt 6) determined the amount of oxygen transmitted through the film. Experiments were done in triplicate. The oxygen permeability was calculated using Equation (5):

$$OP\left(\frac{cm^3\ \mu m}{m^2\ d\ bar}\right) = \frac{P_{O_2} \times V_{cell} \times l}{P_{standard} \times A \times \Delta P_{O_2}} \times \frac{T_{standard}}{T_{measurement}} \tag{5}$$

Where P_{O_2} is the increase in oxygen partial pressure in upper test chamber (hPa d^{-1}), V_{cell} represents the volume of the upper test chamber (116 cm^3), l is the thickness of the film (μm), $P_{standard}$ – Standard pressure (1013 hPa), A is the permeation area (0.0068 m^2), ΔP_{O_2} is the difference in oxygen partial pressure between upper and lower chamber (0.96 bar), $T_{standard}$ is the standard temperature (273 K) and $T_{measurement}$ represents the measured temperature (296 K).

2.6. Tensile properties

The tensile test specimen was prepared by cutting the alginate film using a manual cutting press (ZCP020, Zwick Testing Machines Ltd., Herefordshire, UK) equipped with a cutting die. The tensile dog bone test specimen had an overall length of 35 mm, a gauge length of 10 mm and the narrowest part of the dog bone specimen was 2 mm. Miniaturised tensile test was conducted using a micro-tensile tester (Model MT-200, Deben UK Ltd., Woolpit, UK) equipped with a 200 N load cell. Films were conditioned at 50% RH and placed in a sealed chamber containing a saturated solution of magnesium nitrate hexahydrate, $Mg(NO_3)_2.6H_2O$ (O'Brien, 1948), for a minimum of 3 days prior to testing Prior to the test, two dots were marked on the surface of each dog bone test specimen in the direction of applied load. The strain of the test specimen was then evaluated by monitoring the movement of these two dots using a non-contact optical extensometer (iMetrum Ltd., Bristol, UK). The tensile tests were conducted at a crosshead displacement speed of 1.5 mm min^{-1}. Average results of 8 test specimens were reported for each sample and the strain at break (ε), tensile strength (σ) and tensile modulus (E) calculated.

2.7. Statistical analysis

The response surface methodology (RSM) software package Design Expert 10.0.3 (Stat-Ease Inc., Minneapolis, MN, USA) was used to produce designs to match the response surface models to the experimental data. The experimental data was analyzed using regression analysis and analysis of variance (ANOVA). The linear, quadratic, and interaction terms of the model's regression coefficients, as well as their impacts, were calculated. The F-test was used to determine the significance ($p \leq 0.05$, CI 99.5%). The coefficient of determination (R^2), adjusted coefficient of determination (R^2_{adj}), predicted coefficient of determination (R^2_{pre}) and adequate precision ratio"" were all used to validate the precision of the generated model.

2.8. Model optimization and validation

The optimum process conditions were obtained using Derringer's desirability function (Derringer & Suich, 1980). Additional experimental runs at the model derived concentrations were subsequently carried out to validate the predicted optimization solution. Although, the design carried out was multi-response in nature, responses were evaluated one at time. The accuracy and suitability of the model was then determined by comparing the experimental and predicted values.

2.9. FTIR

FTIR was carried out on the optimum film, disintegrated films and was used to investigate the migration of low molecular weight plasticizers from the alginate composite bioplastic film into the food simulant (distilled water) in the migration study. IR spectra were obtained using a Perkin Elmer Spectrum 400 FT-IR/FT-NIR spectrometer with a universal ATR sampling accessory. The spectra were recorded in the range of 650–4000 cm^{-1} with a 4 cm^{-1} resolution. The IR-laser wavenumber was set at 15780.00 cm^{-1}, OPD velocity of 0.20 cm/s and J-stop size of 8.94 mm.

2.10. TGA

Thermal gravimetric analysis was used to examine the thermal degradation of alginate composite bioplastics that were subjected to the disintegration study". (Discovery TGA, TA Instruments, Elstree, UK). In a N_2 environment, samples weighing about 5 mg were heated from ambient temperature to 700 °C at a rate of 10 °C min^{-1} (50 mL min^{-1}).

2.11. Humidity study

Fabricated and commercial films were conditioned at both 0% and 50 ± 2% relative humidity to investigate the effects on WVP and OP. Films conditioned at 50% RH were placed in a sealed chamber containing a saturated solution of magnesium nitrate hexahydrate, $Mg(NO_3)_2.6H_2O$ (O'Brien, 1948), for a minimum of 3 days prior to testing.

2.12. Disintegration and migration study

Determination of the degree of disintegration of the alginate bioplastic under simulated composting conditions was performed according to the BS EN (2015) standard. The migration study was conducted using according to the European Regulation for food contact materials EU/10/2011. A detailed analysis of the methodology along with relevant equations used can be found in the **Supplementary Material.**

3. Results and discussion

3.1. Statistical analysis

In accordance with the benchmarks designated in Section 2.7 for statistical significance and model adequacy, empirical relationships between the responses (WVP, OP and *E*) and the additives were evaluated.

3.1.1. WVP and OP

Based on the results found for WVP, model indicators ($p = 0.415$) and all model terms ($p > 0.05$) were insignificant. Furthermore, there was a significant Lack of Fit ($p < 0.05$) and all the fit statistics (Adequate Precision = 3.5617, R-squared = 0.5018, $R^2_{adj} = 0.0541$, $R^2_{pre} = -1.6829$) did not meet the desired values for model adequacy. In addition, other transforms (Osborne, 2010), design models (first order, first order with interaction, second order and cubic), were attempted to fit WVP data giving unsatisfactory results. Hence, a statistically sound model for WVP could not be derived and therefore not analyzed. The negative predicted R-squared obtained (−1.6829) gives insight into the model suggesting that a higher order model may gave a better prediction.

For the OP response, a mean model was suggested for model fitting but this only gave a model with an intercept term which statistically could not be used. All other design models and transforms were evaluated and a square root transform for a reduced cubic model-after backward elimination of insignificant factors ($p > 0.05$), were found to give satisfactory model fit statistics (Adequate Precision = 39.8550, R-squared = 0.9953, $R^2_{adj} = 0.9865$, $R^2_{pre} = 0.8442$). However, the Lack of Fit was found to be statistically significant ($p < 0.05$) and thus, showed that the model cannot be used to adequately predict the OP response. The Lack of Fit was significant as this reduced cubic model was 'aliased' and cannot accurately fit within the design. CCD does not contain enough runs to support a full cubic model and cannot uniquely estimate the cubic model parameters (Myers et al., 2009). Higher order models such as special cubic and full cubic models would be required to accurately model the response and this has been reported to occur frequently in mixture experiments -where the order of the required model is higher than that off a second order polynomial (Myers et al., 2009). Ultimately, among all responses considered for this study, *E* was deemed to be the only statistically key performance indicator that can be utilized to navigate the design space.

3.1.2. E

A second order polynomial was effectively fitted to the empirical relationship between *E* and the independent variables. The equation, in terms of coded factors, stipulated for this response via backward elimination of insignificant factors ($p > 0.05$) followed by a transformation was given in Equation (6):

$$Log_{10}(\boldsymbol{E}) = 0.21 + 0.02A + 0.08B + 0.06C + 0.01D - 0.06AB + 0.07A^2 + 0.11C^2 + 0.09D^2 \quad (6)$$

The applied transformation on the response surface design was done to accommodate for curvature in the response function due to interaction with process variables (Osborne, 2010). *E* has linear and quadratic effects linked to the four additives investigated. From Equation (6) and the coefficient for each parameter, it was found that the greatest positive linear effect on the *E* was CMC (B) and the greatest negative effect was the interaction between starch and CMC (AB). The experimental data was analyzed by ANOVA giving the significance level ($p > 0.05$) for each regression coefficient and results presented in Table 3.

A model is considered to be well-fitted to the experimental data if its model p value is significant ($p < 0.05$) while the lack of fit is insignificant ($p > 0.05$) (Hinkelmann & Kempthorne, 2007). The transformed model obtained possessed a high f-value of 10.28 with a low probability ($p < 0.0001$) demonstrating the significance of the model. The Lack of Fit of 1.12 with an accompanying p value of 0.4899 indicated statistical insignificance relative to the pure error ($p > 0.05$) and subsequent diagnosis of residuals showed no abnormalities. Therefore, it can be seen that the fitted model for *E* was well accommodated by the second order polynomial response surface design.

Furthermore, fit statistics were used to evaluate the goodness of fit of the derived model. The coefficient of determination, R^2, was found to be 0.7967. According to Koba, Matsuoka, Osada, and Huang (2007), the R^2 value should be at least 0.80 for the adequacy of the applied regression model. It should be noted that a large value of R^2 does not necessarily imply that the model is a good one and as such the R^2 value obtained from the model was not the only parameter used for evaluation. The difference in the R^2 and adjusted R^2 can be attributed to the inclusion of non-significant terms in the model (Myers et al., 2009). The difference between the R^2_{pred} (0.5262) and R^2_{adj} (0.7192) was less than 0.2, indicating that the model and the data are in reasonable agreement (Anderson & Whitcomb, 2016). Furthermore, adequate precision is determined by the signal-to-noise ratio, with values larger than 4 suggesting adequate model discrimination. The model was determined to have adequate precision of >25, indicating that it is substantial and can be utilized. Thus, the developed model for E was statistically sound and can be used for optimization of the bioplastic composite.

Table 3
Analysis of variance for *E*

Source	Sum of squares	Degree of freedom	Mean square	F value	p value
Model	0.85	8	0.11	10.28	<0.0001
A	0.01	1	0.01	0.86	0.3631[a]
B	0.14	1	0.14	13.62	0.0014
C	0.09	1	0.09	8.60	0.0079
D	0.00	1	0.003	0.25	0.6210[a]
AB	0.06	1	0.06	6.16	0.0216
A^2	0.15	1	0.15	14.45	0.0010
C^2	0.32	1	0.32	31.16	<0.0001
D^2	0.20	1	0.20	19.67	0.0002
Residual	0.22	21	0.01		
Lack of fit	0.17	16	0.01	1.12	0.4899[a]
Pure error	0.05	5	0.01		
Cor Total	1.07	29			
Adeq. prec.	12.6403				
R^2	0.7967				
R^2_{adj}	0.7192				
R^2_{pre}	0.5262				

Note: [a]Not significant ($p > 0.05$).

3.2. Influence of additives on E

The influence of the different additives at varying concentrations on *E* can be seen through the use of 2-D contour plots presented in Fig. 2A–C. The plots illustrate the effect of the concentration of starch (A) and CMC (B) while sorbitol (C) and PEG-200 (D) concentrations are kept constant (at −1, 0 and 1 respectively in terms of coded factors). Two linear coefficients (B and C), three quadratic coefficients (A^2, B^2 and C^2), and only 1 interactive coefficient (AB) were significant. The linear coefficients of A and D were statistically insignificant, and it can be seen that these linear effects had no effect on *E* of the films individually. CMC (B) exhibited a strong positive effect on *E* followed closely by sorbitol (C). CMC and sorbitol as linear positive effects on *E* indicates that the bioplastic film was stiffer and less flexible. This was seen in run 22 where the highest axial point (α) of sorbitol (0.085 g/g) was used which resulted in the highest σ of 91.25 MPa and lowest $\varepsilon$of 4.73% amongst all the runs tested. This is a classic response for CMC as a reinforcement material but not for sorbitol as it behaves as a stiffening agent.

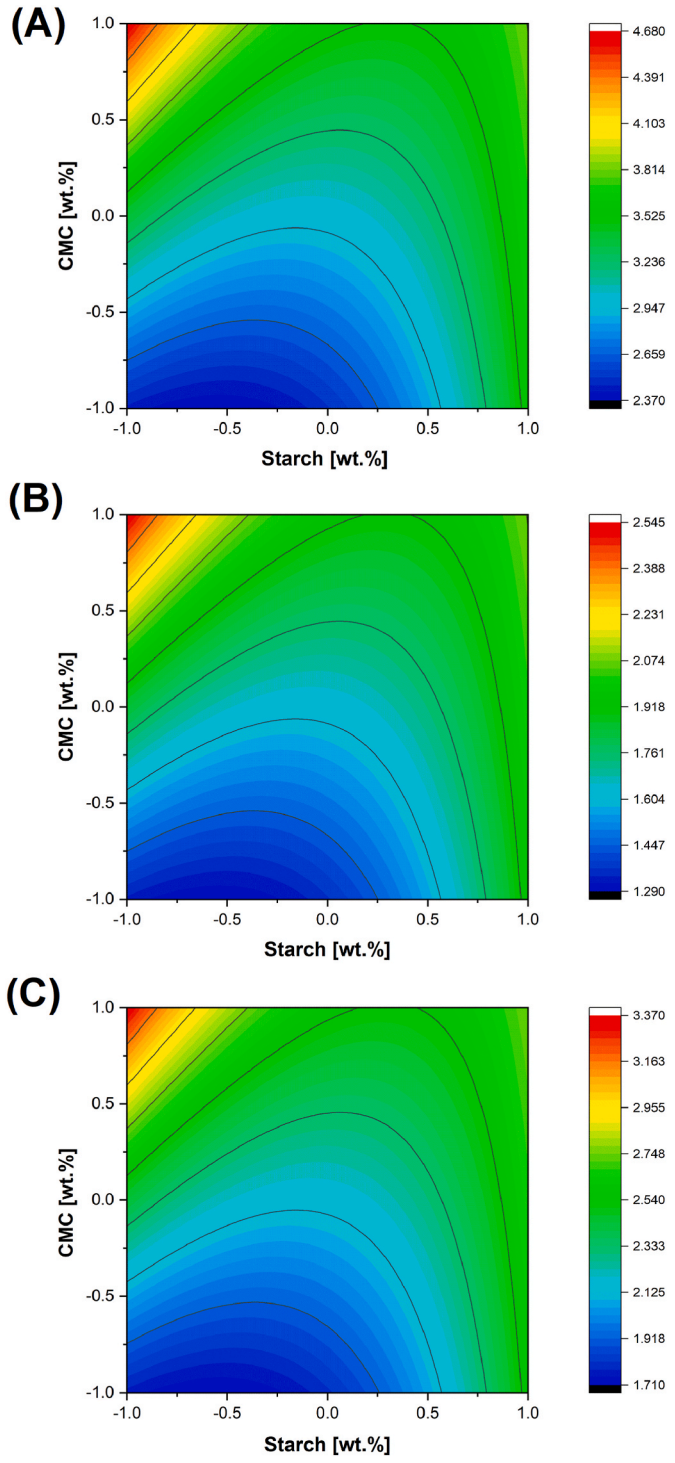

Fig. 2. 2D distribution of E as a function of additive concentration. CMC and starch concentration are the additives shown with the other additives at A) highest, B) midpoint and C) lowest concentration. Colors simulate E responses from blue (lowest) to red (highest). Ranges are A) 2.37–4.68, B) 1.29–2.54 and C) 1.71–3.37. (For interpretation of the references to colour in this figure legend, the reader is referred to the Web version of this article.)

However, starch (A) combined with CMC (B) was found to demonstrate the strongest and only antagonistic effect on *E* of the alginate bioplastic. The combination of these two reinforcement materials characteristically should improve the stiffness owing to a strong intermolecular interaction between the hydroxyl groups of the CMC and starch- with the carboxyl groups of the alginate forming a strong crystalline polymer network accompanying increased hydrogen bonding (Han & Wang, 2017; Lan, He, & Liu, 2018; Rahman, Dafader, & Banu, 2017). However, this was not the case observed in this model. This uncharacteristic response can be ascribed to the high amounts of reinforcement material used exceeding compatibility limits. This resulted in agglomeration within the alginate matrix due to improper dispersion and non-homogeneity. From Fig. 2A it can also be seen that the model stipulates that low starch and high CMC will give the highest *E*and highest stiffness, thus indicating that this would be the best synergistic interaction of the reinforcement material. This further justifies the antagonistic effect seen in Equation **(6)**, attributed to the fact that CMC has a strong affinity for alginate (Putri, Setiawan, & Anggraini, 2018). Furthermore, the crosslinking density and hydrogen bonding of this interaction is poor, leading to a less compact structure and decreased stiffness. Similar effects have been seen in CMC-corn starch films, where high concentrations of both starch and CMC give unfavorable material properties (Rachtanapun, 2009; Tongdeesoontorn, Mauer, Wongruong, Sriburi, & Rachtanapun, 2011; Wahyuningtyas & Dinata, 2018).

From Fig. 2, it can be shown that *E* was at its highest when the concentration of starch was low (0.2 wt%) but all other concentrations were high (0.35 wt% CMC, 0.065 g/g sorbitol and 0.065 g/g PEG 200). As the concentration of the plasticizers decrease to the midpoint (0.045 g/g sorbitol and 0.045 g/g PEG 200), *E* decreases (Fig. 2B), with further reduction to the lowest point resulting in an increase in the *E* (Fig. 2C). At the highest concentration of the plasticizers (0.065 g/g sorbitol and 0.065 g/g PEG 200), 'anti-plasticization' phenomena occurred where the bioplastic has become stiffer and less susceptible to deformation. This was evident from run 27 where the strain at break was 5.15% and the σ was 83.42 MPa- which was among the lowest strain at break values and highest tensile strength value. Anti-plasticization can occur at high plasticizer concentrations leading to enhanced *E* due to a decrease in plasticization (Anderson et al., 1995; Cais, Nozomi, Kawai, & Miyake, 1992). Incorporation of plasticizers increase the free volume and cause molecular mobility within the polymer matrix, which leads to the reorganization of the alginate structure from a flexible to a more ordered crystalline network-resulting in lower deformation (Guerrero, 1989; Lourdin, Bizot, & Colonna, 1997). There are 6 hydroxyl groups present in sorbitol and 2^n in PEG-200 (Antoniou, Liu, Majeed, Qazi, & Zhong, 2014). As plasticizer concentration increased, stronger hydrogen bonding persists between plasticizer-plasticizer interactions over alginate-plasticizer and alginate-alginate units- preventing the motion of polymer chain under stress (reduced elongation). Similar results for this anti-plasticization effect at high concentrations have been reported for sorbitol (Gaudin, Lourdin, Forssell, & Colona, 2000; Suppakul, Chalernsook, Ratisuthawat, Prapasitthi, & Munchukangwan, 2013) and PEG plasticized polymer films (Saberi, Chockchaisawasdee, Golding, Scarlett, & Stathopoulos, 2017).

At midpoint concentrations for CD (0.045 g/g sorbitol and 0.045 g/g PEG 200), the observed decrease in the *E* indicated a relaxed bioplastic model with increased susceptibility to deformation (Fig. 2B). The plasticizing effects were more noticeable at this combination of the polyols. The addition of the plasticizers resulted in a more ductile bioplastic, where the polyols align between alginate molecules and interferes with the intra-molecular forces-leading to the formation of alginate-plasticizer interactions to the detriment of alginate-alginate interactions. This characteristic response can be ascribed to the fact that plasticizers diminish strong intermolecular forces along the polymer matrix and unfastens the structure of the polymer (Sanyang, Sapaun, Jawaid, Ishak, & Sahari, 2015). This is in accordance with other studies using similar polyols (Avella et al., 2007; Gao, Pollet, & Avérous, 2017b; Jost et al., 2014). In comparison to Fig. 2A, it can be shown that the fracture mechanism changes from swift brittle to elastoplastic as the amount of plasticizer increases-resulting in increased elasticity.

At the lowest point of CD (Fig. 2C), the observed increase in *E* suggests higher stiffness and lower deformation. This anti-plasticization phenomena also occurs at low plasticizer concentration, below the threshold where films become stiffer and less flexible (Seow, Cheah, & Chang, 1999). At this low concentration, sorbitol and PEG are not able to position themselves effectively between polymer segments, resulting in insufficient hydrogen bonds within the alginate chains. Authors have reported similar anti-plasticization effects at low concentrations for sorbitol (Aguirre, Borneo, & León, 2013; Chamarthy & Pinal, 2008) and PEG plasticized polymer films (Saberi et al., 2017). Thus, the concentrations of additives proposed in our model can provide benchmarks for obtaining a novel mixed polymer-mixed plasticizer alginate bioplastic.

3.3. Optimization and validation of model results

Derringer's desirability function analysis was used to find the optimum combination of concentrations of additives that targeted an *E* of 3.7 GPa, based on the data obtained and predicted by the model. This target value was achieved by comparing the *E* (GPa) of synthetic polymers PET (2.8–4.1) (Auras, Harte, & Selke, 2004), HDPE (0.8–1.2) (Amjadi & Shah, 2020) and biopolymer PLA (3.5–4.26) (Dizon, Espera, Chen, & Advincula, 2018; Van de Velde & Kiekens, 2002). The concentrations of additives for the optimized bioplastic composite were: 0.263 wt% starch, 0.35 wt% CMC, 0.065 g/g sorbitol and 0.025 g/g PEG 200. The alginate bioplastic composite using these concentrations gave a desirability of 1, where 1 represents maximum tensile properties linked to the target value (Derringer and Suich, 1980). An experimental *E* of 3.93 ± 0.45 GPa (n = 5) was found after fabricating the optimized bioplastic, which was quite similar to the expected model value with an experimental deviation of 6%. Furthermore, a Student's *t*-test (p = 0.05) was carried out and the difference between the model prediction and the experimental values was considered to be statistically insignificant. As a result, the model based on CCD and Derringer's desirability function was successful in predicting the optimal concentration for a bioplastic composite with tensile capabilities similar to PET and PLA.

3.4. FTIR of the optimized alginate film

The FTIR spectra obtained in Fig. 3 indicated intermolecular interactions between the additives in the composite films by shifting of the different functional groups. Firstly, a very broad absorption band in the alginate film at 3600-3000 cm^{-1} is evident- owing to the stretching frequency of the O–H group (Daemi & Barikani, 2012). The O–H band was shifted in the alginate powders (Manugel and *S.natans*) when all additives were blended into the alginate film. This shift indicates intermolecular/intramolecular interactions attributable to the formation of hydrogen bonds between carbonyl and hydroxyl groups (Tong, Xiao, & Lim, 2008). It can be seen that the prominent hydroxyl groups were due to starch, PEG 200 and sorbitol. These additives have good synergy and are well integrated within the polymer matrix during the process of film formation-with water as the solvent hydrating the composite structure. The water present also had an impact on the stretching and deepening of the OH band. Furthermore, the polyols (PEG and sorbitol) in the composite are well known for increasing the intensity of the O–H band in alginate films- owing to the high number of hydroxyl groups present (Gao et al., 2017a; Wang, Zhang, Hu, Yang, & Du, 2007).

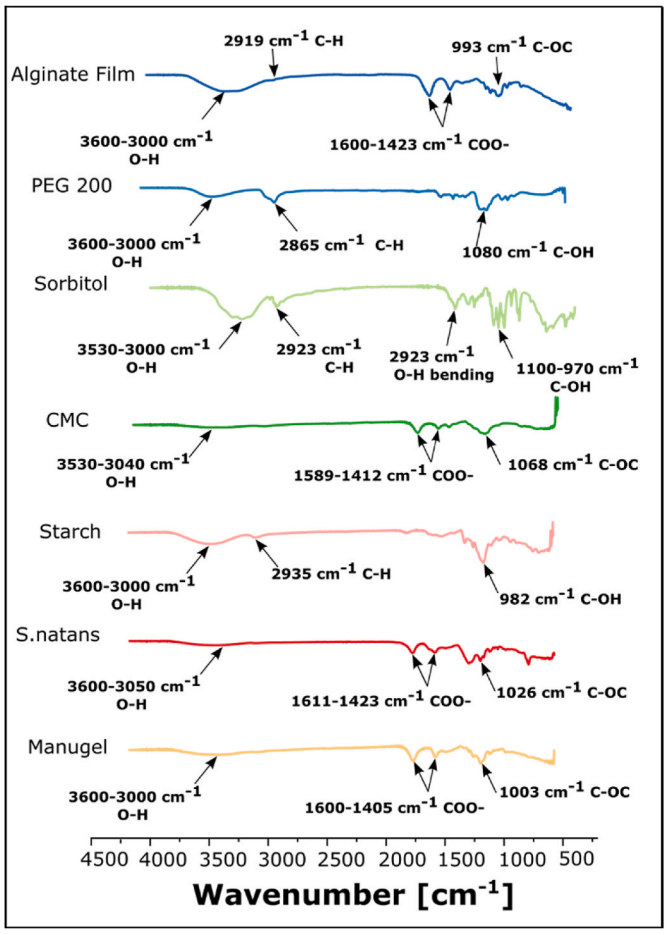

Fig. 3. FTIR spectra of optimum alginate film and additives.

In addition, the spectra of the film showed peaks at around 1600 cm^{-1} and 1423 cm^{-1} attributable to the asymmetric and symmetric vibrations of the COO^{-} groups respectively (Daemi and Barikani, 2012). Blending of carboxylate containing groups within CMC at (1589 cm^{-1} and 1412 cm^{-1}), Manugel (1589 cm^{-1} and 1401 cm^{-1}) and *S.natans* alginate (1599 cm^{-1} and 1401 cm^{-1}) resulted in increased absorption in the COO- band. This indicates vibrations of the C–O and C = O were heightened owing to disruption of intermolecular hydrogen bonds within the polymer matrix.

Additionally, shifts at 1345 cm^{-1} re$^{corded\ for\ the\ alginate\ film,\ was}$ attributed to the C–O stretch in ester bonds produced between the hydroxyl groups in starch, sorbitol and PEG-200 and the carboxylic acids present in CMC and alginate -resulting in a stable structure and good compatibility among additives. Furthermore, shifts at 993 cm^{-1} in the composite were attributed to the C–O stretching vibration of the pyranosyl ring (Daemi and Barikani, 2012). Thus, the FTIR spectra provides good evidence that the alginate, plasticizers and reinforcement material exhibit good molecular affinity and synergy through the establishment of intermolecular interactions.

3.5. Comparison of optimized composite to commercial plastics

3.5.1. E

From Fig. 4A, it can be seen that *E* of the alginate bioplastic composite was comparable to PLA. The *E* was 60% higher than HDPE and 30% lower than of PET. Hence, the alginate composite exhibits similar *E* as PLA and found to be stiffer than HDPE and less deformable than PET. Fig. 4B presents the representative stress-strain curves of the alginate bioplastic, commercial PET, PLA and HDPE samples under uniaxial tension. After the initial elastic response, the alginate bioplastic and commercial PLA samples yielded before failure as evidenced by a sudden load decrease to zero after peak stress was attained. The HDPE and PET samples, however exceeded the limits of the machine after passing the elastic response and did not yield. This high *E* for the alginate compared to HPDE was at the expense of the strain. The strain at break for the alginate film stands at 6.81%, PLA at 43.2% and both HDPE and PET are >60%. These results can guide the application of our alginate bioplastic composite as a food packaging material, where high stiffness is desirable such as with rigid packaging (pouches, trays, cups, containers, and plastic sheets) and cannot be used for applications that require plastic deformations at higher stress levels. Lastly, from Table S2, it was found that the *E* of the alginate bioplastic was amongst the highest for reported alginate sources.

3.5.2. WVP

The WVP of the alginate composite was found to be much higher (2–3 orders of magnitude) than the synthetic plastics as shown in Fig. 4C. This is not an uncommon characteristic, as it is well documented in literature that good barriers to oxygen generally possess molecular structures with hydrogen-bonding forces and polar-polar interactions-resulting in high hydrophilicity and low water vapor barriers (Lagaron, Catalá, & Gavara, 2004; Lee, 1980). Hence, the hydrophilic nature of the composite owing to the presence of hydrophilic functional groups (hydroxyl, carbonyl and carboxyl) from starch, alginate, CMC, sorbitol and PEG-200 in the polymer matrix accounts for these observations. However, it should be noted (from Table S3) that the WVP of our alginate composite was amongst the lowest reported for an alginate film. Thus, from our results, alginate composites can be utilized in food packaging supply chains targeted at low humidity environments.

3.5.3. OP

From Fig. 4D, it can be seen that the most expedient property of the alginate composite is the OP. The value of the OP at 0% and 50 relative humidity was significantly lower (3–4 orders of magnitude) than that of the commercial synthetic and natural polymers. Further to this, it can be seen from Table S4, that the OP for our alginate composite was amongst the lowest reported in literature. Thus, it can be elucidated that the alginate matrix was efficiently cross-linked and uniformly dispersed , resulting in increased tortuosity and lower oxygen diffusion. In addition, resultant interactions and interfacial adhesions between the alginate and the reinforcement materials leads to strong hydrogen bonds, restricting the mobility of the polymer chains and lowering the available free volume for oxygen molecules to diffuse. This further reduces the residence time of the oxygen molecules permeating through the alginate composite films.

Wang et al. (2018) presents a barrier classification of films based on OP and WVP ranging in grades from poor, low, medium, to high and very high. Our results illustrate, for the alginate composite, high barrier to water vapor ($0.46–4.62\ 10^{-12}$ g m/m^2 s Pa) and a very high barrier to oxygen (<0.4 cm^3 µm m^{-2} d^{-1} kPa^{-1}). This classification is the first of its kind for alginate materials and suggests that our alginate bioplastic has excellent potential for active packaging for the protection of perishable goods susceptible to oxygen degradation.

3.5.4. Effect of humidity on WVP and OP

The effects of relative humidity on the WVP of the films tested are presented in Fig. 4C and D. There was an observed increase in the WVP and OP for the alginate film with an increase in relative humidity, which has also been reported for alginate films (Olivas & Barbosa-Cánovas, 2008) and other hydrophilic polysaccharides such as chitosan (Ren, Yan, Zhou, Tong, & Su, 2017), celluloses (Bedane, Ej, Farmahini-Farahani, & Xiao, 2015), starch (Bajpai, Navin, & Ruchi, 2011; Chinma, Ariahu, & Alakali, 2015) and potato peel waste (Othman, Edwal, Risyon, Kadir, & A.Talib, 2017). It is well documented in literature that as the relative humidity increases, the barrier to water vapor and gases of films worsens (Gontard, Guilbert, & Cuq, 1993; McHugh & Krochta, 1994).

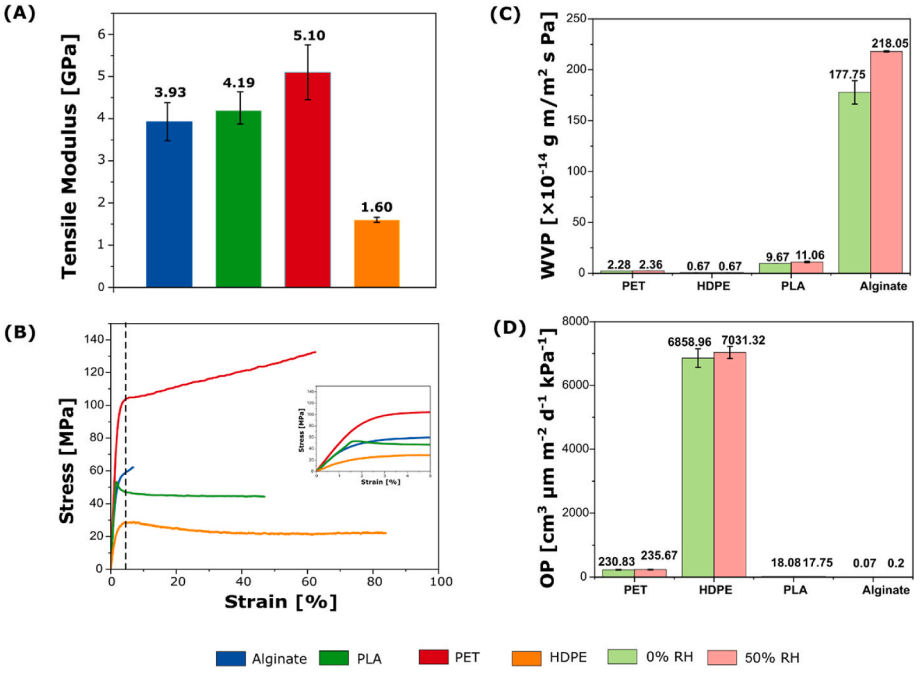

Fig. 4. Overview of material and barrier properties for alginate composite bioplastic and commercial plastic films: A, Tensile Modulus (*E*). B, stress-strain curves. C, WVP at 0 and 50% RH. D, OP at 0 and 50% RH.

Water is a natural plasticizer and thus, films at 50% RH would possess a high availability of water with higher free hydroxyl groups resulting in moisture sorption, a reduction in the intermolecular bonds and increase in the free volume between molecules (Vieira, da Silva, dos Santos, & Beppu, 2011). This free volume accommodates additional sites for more oxygen molecules to permeate through the alginate matrix (Wang et al., 2018). Furthermore, it was seen that changes in the relative humidity of commercial PET, HDPE and PLA had no significant effect on the OP characteristics, rendering the values similar at all levels of RH. This finding was verified by Wang et al. (2018) who observed similar effects for the same synthetic and natural polymers. Due to these findings, the alginate composite packaging would be best suited for low humidity atmospheres.

3.6. Disintegration study

This study investigated the degree of disintegration of composite alginate films under simulated composting conditions. Fig. 5A illustrates the films being degraded over time and it can be seen that the alginate composite visually degraded after 14 days under the simulated conditions. During the first week, increased deformation and opacity was detected-illustrating that hydrolytic degradation process had started. The increased opacity was attributed to changes in the refractive index, linked to water absorption and the formation of low molecular weight compounds through hydrolytic breakdown (Fukushima, Tabuani, Abbate, Arena, & Ferreri, 2010). Furthermore, the increased opacity was as a result of increased crystallinity during degradation. It should be noted that the degradation experiments were carried out at 58 °C, which improve chain mobility (Iglesias-Montes et al., 2021) causing the alginate matrix to crystallize and crack.

This increase in crystallinity and lower thermal stability during degradation has been reported by other authors in the analysis of PCL (Jenkins & Harrison, 2008) and PLA/PHB blends (Iglesias-Montes et al., 2021) in a simulated composting process. However, this increase in crystallinity was not responsible for the lower thermal stability of the degraded samples, but rather attributed to a decrease in the molecular weight of the degraded samples and the preferential degradation of the amorphous regions of the alginate composite.

There was a rapid rate of disintegration during the first 5 days where 64.7% of the initial weight of samples was lost, indicating depolymerization and fragmentation in the biodegradation process as shown in Fig. 5B. During degradation, exoenzymes from aerobic microorganisms break down the complex polymers (starch, cellulose and alginate) resulting in oligomers, dimers and monomers which are used for energy and food (Gu, 2003). The weight loss in the later days (9-14) can be accounted for through the metabolization of the film fragments by microorganisms, indicating mineralization and biomass formation.

In addition to the high rate of degradation, substantial changes were seen in the appearance of the samples. The alginate films were broken down into small pieces owing to the degradation process and fragmentation of the composite film into lower molecular mass. The film after degradation exhibited irregular non-homogenous surfaces with cracks, channels and high porosity-intensified as the degradation elapsed, attributed to microbial activity and hydrolysis. Our results exhibited here follow similar reports on the degradation of PLA using the same standard (BS EN (2015), which was reported to reach 100% of disintegration after 17 days (Bitinis et al., 2013).

3.6.1. FTIR of degraded samples

The FTIR presented in Fig. 5C suggested that there were changes in the chemical structures of the films after degradation. The absorption band at 2919 cm^{-1} attributed to the symmetric and asymmetric stretching vibration of C–H bonds in the aliphatic chains, and the peak at 993 cm^{-1} ascribed to the stretching vibration of the C–O–C bond (Gao et al., 2017b) were all found to have peak shifts in the degraded samples. After 7 days, the C–O–C stretching vibration at 993 cm^{-1} shifted to 1015

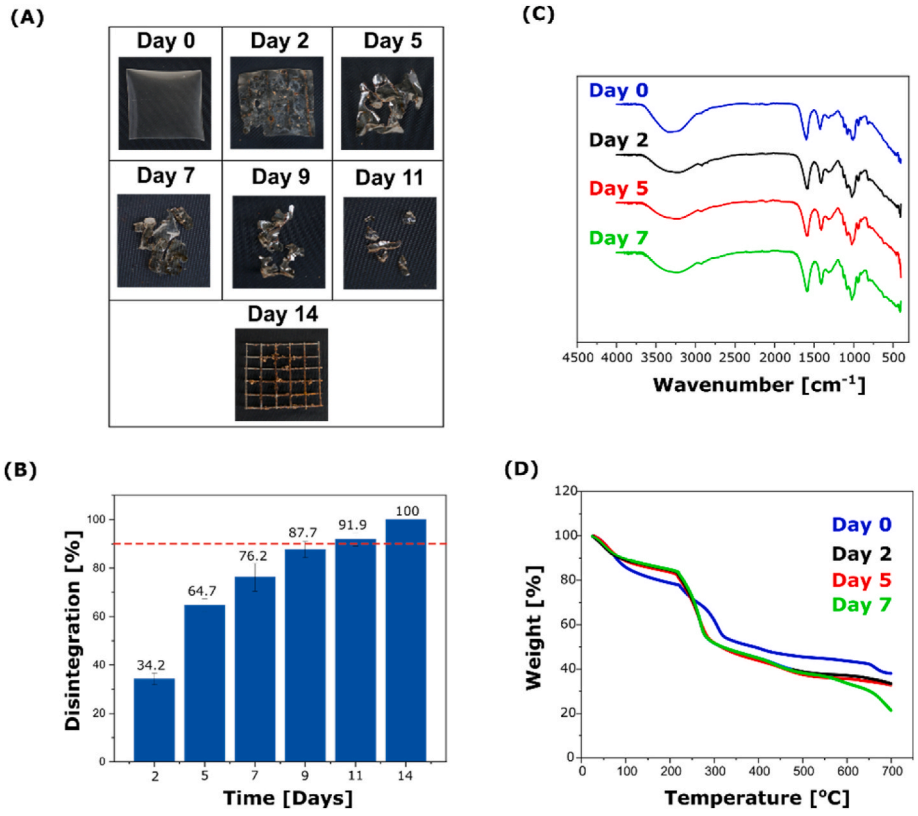

Fig. 5. A, photographs of alginate bioplastic films under disintegration after 14 days. B, percentage disintegration of films after 14 days. C, FTIR spectrum of films after 7 days of disintegration. D, thermogravimetry (TG) curves of films after 7 days.

cm^{-1}-attributed to the breakdown of the polymers and depletion of the oligomer molecules caused by microorganisms, leaving behind highly reactive carboxylate end groups. The C–H bond at 2919 cm^{-1} shifted to 2937 cm^{-1} after 7 days of degradation, ascribed by CH deformation. A further significant observation was seen at around 1600 cm^{-1}, which represents the asymmetric stretching vibration of the $–COO^-$ group (containing the C═O) bond.

This peak shifted to the right as disintegration progressed, to around 1564 cm^{-1} after day 7, which can be explained by the formation of carboxylate ions by aerobic microorganisms and the digestion of starch, cellulose, and alginate on the film's surface. This phenomenon was also reported at around 1600-1603 cm^{-1} for the disintegration of PLA films (Arrieta, López, Rayón, & Jiménez, 2014; Fortunati et al., 2012) and starch films (Zain, Ab Wahab, & Ismail, 2018). Further to this, the peak at 3600-3000 cm^{-1} assigned to the stretching vibrations of O–H bond was found to be broader with stronger intensities after the degradation process. Thus, these results indicate weakened interactions between the polymers and plasticizers in the alginate film matrix, promoting successful disintegration.

3.6.2. TGA of degraded samples

The TG curves presented in Fig. 5D show the alginate composite mass retained after disintegration over 7 days. From the TG curves, it can be seen that the alginate bioplastic composite has a 3-step decomposition process. The first stage can be ascribed to the loss of retained residual water entrapped within the alginate composite, the second stage between 220 and 330 °C associated with the thermal degradation of the polymeric chains in the composite, and the third stage above 330 °C attributed to carbon burning. The second stage degradation temperature is similar to literature where the decomposition temperature of calcium alginate composites was found to be in the range of 208–256 °C (Németh et al., 2018; Sarkar, Sahoo, Das, Prusty, & Swain, 2017; Zhao et al., 2018).

Further to this, the film at day 0 produced the highest mass residue at 37.9% while the film at day 7 possessed the lowest mass residues at 21.4%. It was also seen that as composting proceeded, the thermal decomposition temperature for the alginate composite samples were shifted to lower temperatures. For example, the temperature for the maximum degradation rate for the alginate sample at day 0 shifted from 330 to 298 °C. Thus, the thermal stability of the films decreased significantly while thermal decomposition accelerated as disintegration occurred.

3.7. Migration study

Chemical compounds in the form of plasticizers (PEG-200 and sorbitol) and reinforcement material (starch and CMC) were added to the alginate matrix to improve functionality. However, these chemicals can interact with package components and can migrate-jeopardizing quality assurance and safety (Bhunia, Sablani, Tang, & Rasco, 2013). Thus, a migration study was carried out to evaluate these interactions. Fig. 6 illustrates the FTIR spectra of composite alginate films immersed in distilled water over 10 days. The control was taken as distilled water with no alginate sample present. Results illustrate no observed changes in the FTIR spectra for all samples tested from day 2 to day 10, suggesting that there was no plasticizer or reinforcement material migration occurring. This can be attributed to the strong cross-linked polymeric alginate matrix which effectively encapsulates the plasticizers and reinforcement material. The ionic crosslinking phenomena between Ca^{2+} and diaxially linked guluronic residues in the alginate forms a very compact structure with ionic bridges referred to as the 'egg-box' model (Khalil et al., 2017).

The cross-linking process is referred to as a type of surface modification, resulting in improved water and chemical resistance (Azeredo & Waldron, 2016). This modified surface layer essentially acts as a barrier to migration (Wei, Linde, & Hedenqvist, 2019). Similar results for this

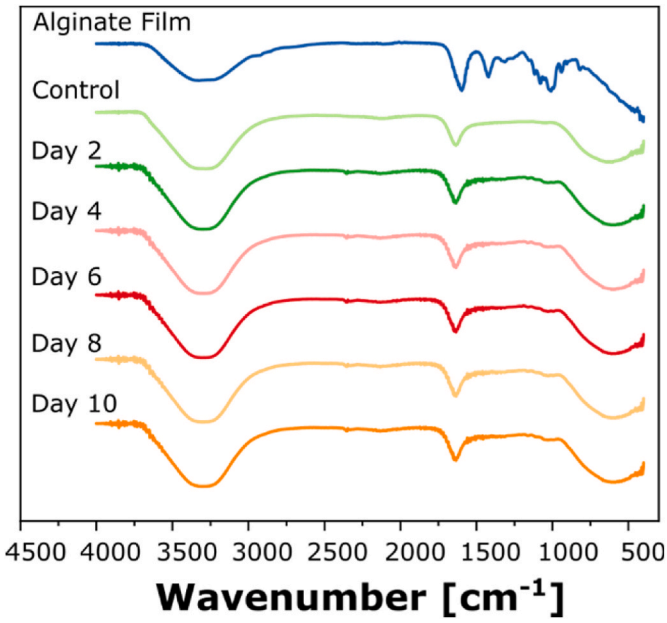

Fig. 6. FTIR spectra of alginate composite immersed in food simulant.

crosslinking effect in plasticizer migration has been reported using crosslinked PVC films (Ambrogi, Brostow, Carfagna, Pannico, & Persico, 2012; Lakshmi & Jayakrishnan, 1998). Therefore, our alginate bioplastics meets the EU standard (EU 10/2011) for overall migration, specifically for any long term storage at room temperature or below, including heating up to 70 °C for up to 2 h, or heating up to 100 °C for up to 15 min. Thus, this migration study can guide the production of novel safe composite alginate bioplastics for active packaging applications.

Ultimately, our study presents the foundation of optimized alginate films for packaging applications and informs on future models, utilizing additional responses to improve the experimental design; such as glass transition temperature (T_g) and contact angle to investigate critical chemical indicators such as crystallinity, hydrophilicity and flexibility.

4. Conclusions

The work presented in this study illustrates the potential of a novel alginate composite bioplastic derived from waste *Sargassum natans*. The alginate composite was optimized through the use of an RSM design using DoE-giving an optimum film formulation of 6 wt% alginate, 0.263 wt% starch, 0.35 wt% CMC, 0.065 g/g sorbitol and 0.025 g/g PEG 200. The composite films possess ultra-low OP (0.2 cm^3 μm m^{-2} d^{-1} kPa^{-1}), good WVP (2.18 × 10^{-12} g m/m^2 s Pa) and high *E* of 3.93 GPa. Furthermore, alginate composite films were characterized and compared to commercial HDPE, PET and PLA and were found to have better OP, higher WVP and comparable material properties. Our results also illustrate that the alginate composite degrades in simulated compost after 14 days and the additives within the composite material do not migrate -thus making it safe for use as a food packaging alternative in low moisture environments.

CRediT authorship contribution statement

Akeem Mohammed: Methodology, Investigation, Visualization, Writing – original draft, Writing – review & editing, 2. **Andre Gaduan:** Methodology, Investigation, Data curation, Investigation, Writing – original draft. **Pooran Chaitram:** Data curation, Investigation. **Anaadi Pooran:** Data curation, Investigation. **Koon-Yang Lee:** Methodology, Investigation, Visualization, Validation, Writing – review & editing. **Keeran Ward:** Methodology, Investigation, Visualization, Supervision, Project administration, Validation, Formal analysis, Funding

acquisition, Writing – review & editing.

Declaration of competing interest

The authors declare that they have no known competing financial interests or personal relationships that could have appeared to influence the work reported in this paper.

Data availability

Data will be made available on request.

Acknowledgements

This work was supported by a University of the West Indies, St. Augustine Campus-Trinidad and Tobago Research and Development Impact Fund Innovation Proof of Concept Grant-26607. The authors would like to thank Trishana Ramgoolie, Idris Mohammed, Jodi Porter and Maria Jimenez-Solomon for their contributions in developing the foundation for the production of alginate bioplastic composites.

Appendix A. Supplementary data

Supplementary data to this article can be found online at https://doi.org/10.1016/j.foodhyd.2022.108192.

References

Aguirre, A., Borneo, R., & León, A. E. (2013). Properties of triticale protein films and their relation to plasticizing–antiplasticizing effects of glycerol and sorbitol. *Industrial Crops and Products, 50*, 297–303.

Ambrogi, V., Brostow, W., Carfagna, C., Pannico, M., & Persico, P. (2012). Plasticizer migration from cross-linked flexible PVC: Effects on tribology and hardness. *Polymer Engineering & Science, 52*(1), 211–217.

Amjadi, M., & Shah, H. (2020). Tensile behavior of high-density polyethylene including the effects of processing technique, thickness, temperature, and strain rate. *Polymers, 12*, 1–14.

Anderson, S. L., Grulke, E. A., DeLassus, P. T., Smith, P. B., Kocher, C. W., & Landes, B. G. (1995). A model for antiplasticization in polystyrene. *Macromolecules, 28*(8), 2944–2954.

Anderson, M., & Whitcomb, P. (2016). *RSM simplified: Optimizing processes using response surface methods for design of experiments* (2nd ed.). New York: CRC Press.

Antoniou, J., Liu, F., Majeed, H., Qazi, H. J., & Zhong, F. (2014). Physicochemical and thermomechanical characterization of tara gum edible films: Effect of polyols as plasticizers. *Carbohydrate Polymers, 111*, 359–365.

Arrieta, M. P., López, J., Rayón, E., & Jiménez, A. (2014). Disintegrability under composting conditions of plasticized PLA–PHB blends. *Polymer Degradation and Stability, 108*, 307–318.

ASTM, A. S. f. T. a. M. (1995). *E95-96 standard test methods for water vapor transmission of materials*.

ASTM, A. S. f. T. a. M. (2017). *ASTM d3985-17, standard test method for oxygen gas transmission rate through plastic film and sheeting using a coulometric sensor*.

Auras, R., Harte, B., & Selke, S. (2004). An overview of polylactides as packaging materials. *Macromolecular Bioscience, 4*(9), 835–864.

Avella, M., Pace, E. D., Immirzi, B., Impallomeni, G., Malinconico, M., & Santagata, G. (2007). Addition of glycerol plasticizer to seaweeds derived alginates: Influence of microstructure on chemical–physical properties. *Carbohydrate Polymers, 69*(3), 503–511.

Azeredo, H. M. C., Miranda, K. W. E., Rosa, M. F., Nascimento, D. M., & de Moura, M. R. (2012). Edible films from alginate-acerola puree reinforced with cellulose whiskers. *LWT - Food Science and Technology, 46*(1), 294–297.

Azeredo, H. M. C., & Waldron, K. W. (2016). Crosslinking in polysaccharide and protein films and coatings for food contact – a Review. *Trends in Food Science & Technology, 52*, 109–122.

Bajpai, S., Navin, C., & Ruchi, L. (2011). Water vapor permeation and antimicrobial properties of sago starch based films formed via microwave irradiation. *International Food Research Journal, 18*, 417–426.

Bedane, A. H., Ej, M., Farmahini-Farahani, M., & Xiao, H. (2015). Water vapor transport properties of regenerated cellulose and nanofibrillated cellulose films. *Journal of Membrane Science, 493*, 46–57.

Bhunia, K., Sablani, S. S., Tang, J., & Rasco, B. (2013). Migration of chemical compounds from packaging polymers during microwave, conventional heat treatment, and storage. *Comprehensive Reviews in Food Science and Food Safety, 12*(5), 523–545.

Bitinis, N., Fortunati, E., Verdejo, R., Bras, J., Kenny, J. M., Torre, L., et al. (2013). Poly (lactic acid)/natural rubber/cellulose nanocrystal bionanocomposites. Part II: Properties evaluation. *Carbohydrate Polymers, 96*(2), 621–627.

Cais, R. E., Nozomi, M., Kawai, M., & Miyake, A. (1992). Antiplasticization and abrasion resistance of polycarbonates in the charge-transport layer of an organic photoconductor. *Macromolecules, 25*(18), 4588–4596.

Chamarthy, S. P., & Pinal, R. (2008). Plasticizer concentration and the performance of a diffusion-controlled polymeric drug delivery system. *Colloids and Surfaces A: Physicochemical and Engineering Aspects, 331*(1), 25–30.

Chia, W. Y., Ying Tang, D. Y., Khoo, K. S., Kay Lup, A. N., & Chew, K. W. (2020). Nature's fight against plastic pollution: Algae for plastic biodegradation and bioplastics production. *Environmental Science and Ecotechnology, 4*, Article 100065.

Chinma, C. E., Ariahu, C. C., & Alakali, J. S. (2015). Effect of temperature and relative humidity on the water vapour permeability and mechanical properties of cassava starch and soy protein concentrate based edible films. *Journal of Food Science & Technology, 52*(4), 2380–2386.

Daemi, H., & Barikani, M. (2012). Synthesis and characterization of calcium alginate nanoparticles, sodium homopolymannuronate salt and its calcium nanoparticles. *Scientia Iranica, 19*(6), 2023–2028.

Derringer, G., & Suich, R. (1980). Simultaneous optimization of several response variables. *Journal of Quality Technology, 12*(4), 214–219.

Dizon, J. R. C., Espera, A. H., Chen, Q., & Advincula, R. C. (2018). Mechanical characterization of 3D-printed polymers. *Additive Manufacturing, 20*, 44–67.

EN, B. S. E. B.. (2015). *Plastics — determination of the degree of disintegration of plastic materials under simulated composting conditions in a laboratory-scale test* (p. 7).

Fortunati, E., Armentano, I., Iannoni, A., Barbale, M., Zaccheo, S., Scavone, M., et al. (2012). New multifunctional poly(lactide acid) composites: Mechanical, antibacterial, and degradation properties. *Journal of Applied Polymer Science, 124*(1), 87–98.

Fukushima, K., Tabuani, D., Abbate, C., Arena, M., & Ferreri, L. (2010). Effect of sepiolite on the biodegradation of poly(lactic acid) and polycaprolactone. *Polymer Degradation and Stability, 95*(10), 2049–2056.

Gao, C., Pollet, E., & Avérous, L. (2017a). Innovative plasticized alginate obtained by thermo-mechanical mixing: Effect of different biobased polyols systems. *Carbohydrate Polymers, 157*, 669–676.

Gao, C., Pollet, E., & Avérous, L. (2017b). Properties of glycerol-plasticized alginate films obtained by thermo-mechanical mixing. *Food Hydrocolloids, 63*, 414–420.

Gaudin, S., Lourdin, D., Forssell, P., & Colona, P. (2000). Antiplasticisation and oxygen permeability of starch-sorbitol films. *Carbohydrate Polymers, 43*, 33–37.

Gontard, N., Guilbert, S., & Cuq, J.-L. (1993). Water and glycerol as plasticizers affect mechanical and water vapor barrier properties of an edible wheat gluten film. *Journal of Food Science, 58*(1), 206–211.

Gu, J.-D. (2003). Microbiological deterioration and degradation of synthetic polymeric materials: Recent research advances. *International Biodeterioration & Biodegradation, 52*(2), 69–91.

Guerrero, S. J. (1989). Antiplasticization and crystallinity in poly(vinyl chloride). *Macromolecules, 22*(8), 3480–3485.

Han, Y., & Wang, L. (2017). Sodium alginate/carboxymethyl cellulose films containing pyrogallic acid: Physical and antibacterial properties. *Journal of the Science of Food and Agriculture, 97*(4), 1295–1301.

Hinkelmann, K., & Kempthorne, O. (2007). *Design and analysis of experiments* (2nd ed.). New Jersey: John Wiley & Sons.

Ho, B. K., Azahari, B., Yhaya, M. F., Talebi, A., Ng, C. W., Tajarudin, H. A., et al. (2020). Green technology approach for reinforcement of calcium chloride cured sodium alginate films by isolated bacteria from palm oil mill effluent (POME). *Sustainability, 12*(22), 1–13.

Iglesias-Montes, M. L., Soccio, M., Luzi, F., Puglia, D., Gazzano, M., Lotti, N., et al. (2021). Evaluation of the factors affecting the disintegration under a composting process of poly(lactic acid)/Poly(3-hydroxybutyrate) (PLA/PHB) blends. *Polymers, 13*(18).

Jenkins, M. J., & Harrison, K. L. (2008). The effect of crystalline morphology on the degradation of polycaprolactone in a solution of phosphate buffer and lipase. *Polymers for Advanced Technologies, 19*(12), 1901–1906.

Johnson, D., Ko, D., Franks, J., Moreno, P., & Sanchez-Rubio, G. (2012). The Sargassum invasion of the eastern caribbean and dynamics of the equatorial north atlantic. In *Proceedings of the 65th Gulf and Caribbean fisheries institute* (pp. 102–103). Columbia.

Jost, V., Kobsik, K., Schmid, M., & Noller, K. (2014). Influence of plasticiser on the barrier, mechanical and grease resistance properties of alginate cast films. *Carbohydrate Polymers, 110*, 309–319.

Kaiser, K., Schmid, M., & Schlummer, M. (2018). Recycling of polymer-based multilayer packaging: A Review. *Recycling, 3*(1), 1.

Khalil, A., Tye, Y., Saurabh, C., Peng, L. C., Lai, T. K., Chong, E. W. N., et al. (2017). *Biodegradable polymer films from seaweed polysaccharides: A Review on cellulose as a reinforcement material, 11*.

Koba, K., Matsuoka, A., Osada, K., & Huang, Y.-S. (2007). Effect of loquat (*Eriobotrya japonica*) extracts on LDL oxidation. *Food Chemistry, 104*(1), 308–316.

Lagaron, J. M., Catalá, R., & Gavara, R. (2004). Structural characteristics defining high barrier properties in polymeric materials. *Materials Science and Technology, 20*(1), 1–7.

Lakshmi, S., & Jayakrishnan, A. (1998). Photocross-linking of dithiocarbamate-substituted PVC reduces plasticizer migration. *Polymer, 39*(1), 151–157.

Langin, K. (2018). Seaweed masses assault caribbean islands. *Science, 360*(6394), 1157–1158.

Lan, W., He, L., & Liu, Y. (2018). *Preparation and properties of sodium carboxymethyl cellulose/sodium alginate/chitosan composite film. 8*.

Lee, W. M. (1980). Selection of barrier materials from molecular structure. *Polymer Engineering & Science, 20*(1), 65–69.

Li, J., He, J., Huang, Y., Li, D., & Chen, X. (2015). Improving surface and mechanical properties of alginate films by using ethanol as a Co-solvent during external gelation. *Carbohydrate Polymers, 123*, 208–216.
Liley, P. E., Thomson, G. H., Friend, D., Daubert, T., & Buck, E. (2008). Physical and chemical data. In D. W. Green, & R. H. Perry (Eds.), *Perry's chemical engineers' handbook* (8th ed., pp. 1–374). New York: McGraw-Hill Education.
Lim, J.-Y., Hii, S.-L., Chee, S.-Y., & Wong, C.-L. (2018). *Sargassum siliquosum* J. Agardh extract as potential material for synthesis of bioplastic film. *Journal of Applied Phycology, 30*, 3285–3297.
Lourdin, D., Bizot, H., & Colonna, P. (1997). "Antiplasticization" in starch-glycerol films? *Journal of Applied Polymer Science, 63*(8), 1047–1053.
Marrone, M., & Tamarindo, S. (2018). *Paving the sustainability journey: Flexible packaging between circular economy and resource efficiency*.
McHugh, T. H., & Krochta, J. M. (1994). Sorbitol- vs glycerol-plasticized whey protein edible films: Integrated oxygen permeability and tensile property evaluation. *Journal of Agricultural and Food Chemistry, 42*(4), 841–845.
Murad, M., Karim, A., Bhat, R., Uthumporn, U., & Chew, S. (2011). Physical and mechanical properties of sago starch - alginate films incorporated with calcium chloride. *International Food Research Journal, 18*(3), 1027–1033.
Myers, R. H., Montgomery, D. C., & Anderson-Cook, C. M. (2009). *Response surface methodology: Process and product optimization using designed experiments* (4th ed.). New Jersey: Wiley.
Németh, B., Németh, Á. S., Ujhidy, A., Tóth, J., Trif, L., Gyenis, J., et al. (2018). Fully bio-originated latent heat storing calcium alginate microcapsules with high coconut oil loading. *Solar Energy, 170*, 314–322.
O'Brien, F. E. M. (1948). The control of humidity by saturated salt solutions. *Journal of Scientific Instruments, 25*(3), 73–76.
Olivas, G., & Barbosa-Cánovas, G. (2008). Alginate–calcium films: Water vapor permeability and mechanical properties as affected by plasticizer and relative humidity. *LWT - Food Science and Technology, 41*, 359–366.
Osborne, J. (2010). Improving your data transformations: Applying the box-cox transformation. *Practical Assessment, Research and Evaluation, 15*.
Othman, S., Edwal, S., Risyon, N., Kadir, R., & Talib, R. A. (2017). Water sorption and water permeability properties of edible film made from potato peel waste. *Food Science and Technology, 37*, 63–70.
Pilz, H., Brandt, B., & Fehringer, R. (2010). *The impact of plastics on life cycle energy consumption and greenhouse gas emissions in Europe*. Austria.
Putri, D., Setiawan, A., & Anggraini, P. (2018). Physical properties of edible sorgum starch film added with carboxymethyl cellulose. *Journal of Physical Science, 29*, 185–194.
Rachtanapun, P. (2009). Blended films of carboxymethyl cellulose from papaya peel (CMCp) and corn starch. *Natural Science, 43*, 259–266.
Rahman, N., Dafader, C., & Banu, P. (2017). Preparation and property analysis of biodegradable packaging film from alginate, starch and citric acid. *Journal of Polymer Science and Technology, 2*(1), 20–35.
Ren, L., Yan, X., Zhou, J., Tong, J., & Su, X. (2017). Influence of chitosan concentration on mechanical and barrier properties of corn starch/chitosan films. *International Journal of Biological Macromolecules, 105*, 1636–1643.
Resiere, D., Valentino, R., Nevière, R., Banydeen, R., Gueye, P., Florentin, J., et al. (2018). *Sargassum* seaweed on caribbean islands: An international public health concern. *The Lancet, 392*(10165), 2691.
Rhim, J.-W. (2004). Physical and mechanical properties of water resistant sodium alginate films. *LWT - Food Science and Technology, 37*(3), 323–330.
Saberi, B., Chockchaisawasdee, S., Golding, J. B., Scarlett, C. J., & Stathopoulos, C. E. (2017). Physical and mechanical properties of a new edible film made of pea starch and guar gum as affected by glycols, sugars and polyols. *International Journal of Biological Macromolecules, 104*, 345–359.
Sanyang, M., Sapaun, S., Jawaid, M., Ishak, M., & Sahari, J. (2015). Effect of plasticizer type and concentration on physical properties of biodegradable films based on sugar palm (*Arenga pinnata*) starch for food packaging. *Journal of Food Science & Technology, 53*(1), 326–336.
Sarkar, N., Sahoo, G., Das, R., Prusty, G., & Swain, S. K. (2017). Carbon quantum dot tailored calcium alginate hydrogel for pH responsive controlled delivery of vancomycin. *European Journal of Pharmaceutical Sciences, 109*, 359–371.
Seow, C. C., Cheah, P. B., & Chang, Y. P. (1999). Antiplasticization by water in reduced-moisture food systems. *Journal of Food Science, 64*(4), 576–581.
Soares, C. T.d. M., Ek, M., Östmark, E., Gällstedt, M., & Karlsson, S. (2022). Recycling of multi-material multilayer plastic packaging: Current trends and future scenarios. *Resources, Conservation and Recycling, 176*, Article 105905.
Suppakul, P., Chalernsook, B., Ratisuthawat, B., Prapasitthi, S., & Munchukangwan, N. (2013). Empirical modeling of moisture sorption characteristics and mechanical and barrier properties of cassava flour film and their relation to plasticizing–antiplasticizing effects. *LWT - Food Science and Technology, 50*(1), 290–297.
Tongdeesoontorn, W., Mauer, L. J., Wongruong, S., Sriburi, P., & Rachtanapun, P. (2011). Effect of carboxymethyl cellulose concentration on physical properties of biodegradable cassava starch-based films. *Chemistry Central Journal, 5*(6), 1–8.
Tong, Q., Xiao, Q., & Lim, L.-T. (2008). Preparation and properties of pullulan–alginate–carboxymethylcellulose blend films. *Food Research International, 41*(10), 1007–1014.
Van Eygen, E., Laner, D., & Fellner, J. (2018). Circular economy of plastic packaging: Current practice and perspectives in Austria. *Waste Manag, 72*, 55–64.
Van de Velde, K., & Kiekens, P. (2002). Biopolymers: Overview of several properties and consequences on their applications. *Polymer Testing, 21*(4), 433–442.
Vieira, M. G. A., da Silva, M. A., dos Santos, L. O., & Beppu, M. M. (2011). Natural-based plasticizers and biopolymer films: A Review. *European Polymer Journal, 47*(3), 254–263.
Wahyuningtyas, D., & Dinata, A. (2018). Combination of carboxymethyl cellulose (CMC) - corn starch edible film and glycerol plasticizer as a delivery system of diclofenac sodium. *AIP Conference Proceedings, 1977*, Article 030032.
Wang, L., Auty, M. A. E., & Kerry, J. P. (2010). Physical assessment of composite biodegradable films manufactured using whey protein isolate, gelatin and sodium alginate. *Journal of Food Engineering, 96*(2), 199–207.
Wang, J., Gardner, D. J., Stark, N. M., Bousfield, D. W., Tajvidi, M., & Cai, Z. (2018). Moisture and oxygen barrier properties of cellulose nanomaterial-based films. *ACS Sustainable Chemistry & Engineering, 6*(1), 49–70.
Wang, Q., Zhang, N., Hu, X., Yang, J., & Du, Y. (2007). Alginate/polyethylene glycol blend fibers and their properties for drug controlled release. *Journal of Biomedical Materials Research Part A, 82A*(1), 122–128.
Wei, X.-F., Linde, E., & Hedenqvist, M. S. (2019). Plasticiser loss from plastic or rubber products through diffusion and evaporation. *Npj Materials Degradation, 3*(1), 1–18.
Zain, A. H. M., Ab Wahab, M. K., & Ismail, H. (2018). Biodegradation behaviour of thermoplastic starch: The roles of carboxylic acids on cassava starch. *Journal of Polymers and the Environment, 26*(2), 691–700.
Zeller, M. A., Hunt, R., Jones, A., & Sharma, S. (2013). Bioplastics and their thermoplastic blends from spirulina and chlorella microalgae. *Journal of Applied Polymer Science, 130*(5), 3263–3275.
Zhao, W., Qi, Y., Wang, Y., Xue, Y., Xu, P., Li, Z., et al. (2018). Morphology and thermal properties of calcium alginate/reduced graphene oxide composites. *Polymers, 10*(9), 1–11.
Zygmunt, J. (2007). In Waterwise (Ed.), *Hidden waters* (pp. 1–35). UK.